$NaPO_3$-AlF_3 GLASSES: FLUORINE EVAPORATION DURING MELTING AND THE RESULTING VARIATIONS IN STRUCTURE AND PROPERTIES

Doris Möncke[1,2*], Manoel da Cruz Barbosa Neto[2], Henrik Bradtmüller[3], Gabriel Buzatto de Souza[2], Alisson M. Rodrigues[2], Hager S. Elkholy[4], Hosam A. Othman[4], Benjamin J.A. Moulton[5], Efstratios I. Kamitsos[1], Ana Candida M. Rodrigues[2], Doris Ehrt[6]

[1]*Theoretical and Physical Chemistry Institute, National Hellenic Research Foundation, 48 Vassileos Constantinou Avenue, 11635 Athens, Greece*
[2]*LaMaV, Laboratório de Materiais Vítreos, Departamento de Engenharia de Materiais, Universidade Federal de São Carlos, Rod. Washington Luis, km 235 - São Carlos - SP. Postal code: 13565-905, Brazil*
[3]*Institut für Physikalische Chemie, WWU Münster, Corrensstraße 30, D48149 Münster, Germany*
[4]*Physics Department, Faculty of Science, Menoufia University, Shebin El-Koom, Egypt, Postal code:32511*
[5]*Departamento de Física, Universidade Federal de São Carlos, Brazil Rod. Washington Luis, Km 235 13565-905 São Carlos, SP, Brazil*
[6]*Otto-Schott-Institut für Glaschemie, Friedrich-Schiller-Universität, Fraunhoferstr. 6, 07743 Jena, Germany (retired)*
**moencke@alfred.edu; current: Alfred University, Inamori School of Engineering, 1 Saxon Drive, Alfred, NY 14802, USA*

Received 15 November 2017
Accepted 15 June 2018

ABSTRACT

Four glass series with identical nominal composition of (100-x)$NaPO_3$-xAlF_3 (NAPF), with x = 0 to 40 mol %, were prepared by melting under different conditions and are compared here for their compositional and structural variations. Melting these glasses at different temperatures, with or without a crucible lid, with or without an additional fluorinating agent (NH_4HF_2 or NH_4F) and with different quality of the raw materials (OH content) was found to determine fluoride retention. In addition, melting in alumina crucibles can change the glass composition through Al_2O_3 uptake from the crucible, which does not happen to melts prepared in Pt crucibles. Glasses of the differently prepared series were investigated for their actual composition and in regard to structural variations using Raman and also solid-state NMR spectroscopy. The glass density increases for all series in a similar manner with increasing fraction of AlF_3. The glass transition temperatures T_g vary by up to 100°C between nominally similar glasses prepared under different conditions. A higher T_g is generally observed for higher aluminum content and lower fluoride levels. Thus, glasses melted in Al_2O_3 crucibles have the highest F-loss and showed the highest T_g values. The effect of the melting temperature is reflected in the number of P-F bonds which break up in NAPF glasses above 850°C, while Al-F bonds are more stable.

Keywords: Raman Spectroscopy, fluorophosphate, fluoride-phosphate, NMR spectroscopy, F-loss.

INTRODUCTION

Fluoro-aluminate based phosphate glasses are interesting optical materials, which combine the advantages of fluoride glasses, such as low polarizability, low refractive index, positive partial dispersion and high transparency in the UV to IR wavelength region, with the advantages of phosphate glasses such as better glass forming ability and high solubility for active dopants, like rare earth ions [1, 2]. Varying the fluoroaluminate to phosphate ratio allows tuning of many glass properties. Some fluoride-phosphate glass systems have been

optimized for optical applications for instance optical lenses, laser glasses or fluorescence standards [1, 2]. However, their complex composition, which goes beyond the binary AlF_3/phosphate composition, contains additional fluorides i.e. MgF_2, CaF_2 and SrF_2. The structural investigation of these glasses is consequently extremely more complicated [3 - 6], while the simpler AlF_3-$NaPO_3$ system (NAPF) offers better opportunities for structural studies [6, 7].

Generally, the structure of NAPF glasses consists predominantly of metaphosphate chains and $Al(O,F)_6$ polyhedra. Oxygen atoms link phosphate and fluoro-aluminate groups, while sodium ions cross-link through their coordination to fluoride and oxygen atoms. Both oxygen and fluoride ions can bond to phosphate and aluminate groups, while only oxygen atoms can link any combination of P and Al atoms. Previous NMR experiments identified Al-F-Al but no P-F-Al bridges, however, most fluorine atoms were found in terminal P-F or Al-F bonds [6, 7]. Increasing AlF_3 contents breaks the metaphosphate chains and forms more pyrophosphate units [6, 8]. It is noted that oxygen uptake from the atmosphere and fluoride loss cannot be fully prevented when melting under air, but can be reduced substantially by choosing an appropriate set up as detailed below.

The various parameter most important for a high fluorine retention will be presented and discussed in the following in more detail for four nominally identical NAPF series (*series I, II, III,* and *IV*). The four series were melted from different batches of raw materials (especially the water content of $NaPO_3$ or the F/OH content of AlF_3 is of concern) and under various conditions. For example, melting with or without a crucible lid, using platinum or Al_2O_3 crucibles or varying melting temperatures, and even the humidity of the atmosphere can impact evaporation losses and the final glass composition. The actual glass composition was analysed by SEM-EDX, and for *series I* the F-content was further determined by wet chemical analysis. Raman spectroscopy was used to probe structural variations as a function of preparation conditions and solid-state nuclear magnetic resonance (NMR) was employed for selected specimens to characterize possible changes in the next nearest neighbour environments of Al. Compositional and structural changes were finally correlated to selected physical properties such as density, glass transition temperature and refractive index.

EXPERIMENTAL

Glass preparation

Glass samples of the nominal composition (100-x) $NaPO_3$-xAlF_3 with x = 0 to 40, were prepared by standard melt-cooling technology [6, 7]. Powdered optical grade Na_2CO_3, $(NH_4)_2HPO_4$, $NaPO_3$, AlF_3, and NH_4F, as well as NH_4HF_2 were used as raw materials. Four glass series with identical nominal compositions, but with different melt histories were investigated and are compared in this study. Table 1 lists the differences in the preparation of each *series I to IV* for glasses NAPF-X (X = 0, 10, 20, 30 and 40). The data for *series III* are taken from Le et al. [8].

$NaPO_3$ glass

For *series II*, $NaPO_3$ glass was prepared from Na_2CO_3 and $(NH_4)_2HPO_4$ in alumina crucibles. 50 g batches were placed into a muffle furnace, heated to 750°C with a heating rate of 30°C/min, and then melted for 60 minutes at 790°C. Part of the melt was poured into graphite moulds, while the rest of the melt was splat quenched. The quenched $NaPO_3$ glass was afterwards powdered for reuse as $NaPO_3$ source in the preparation of the NAPF glasses of *series II*.

For series I, III and *IV,* $NaPO_3$ powder was used in the preparation of $NaPO_3$ glasses, using either SiO_2 crucibles as in *series I* and *III* (100 g), or Al_2O_3 crucibles in *series IV* (10 g). *Glass I* was melted at 800°C for 60 min, *glass III* at 800°C for 90 min [8], and *glass IV* was melted at 1000°C for 60 min.

NAPF glasses

NAPF glasses of the series (100-x)$NaPO_3$-xAlF_3 with x = 10 to 40 (in mol %), were prepared from commercial AlF_3 and crystalline $NaPO_3$ powder (*I, III, IV*) or powdered $NaPO_3$ glass (*II*). As the available Fluoride content might be affected by the quality of employed AlF_3, it was analyzed priore to synthesis by wet chemical analysis and SEM - EDX for *series I* and *II* respectively and yielded 60 - 62 mass % consistently for both series. The addition of several mass % $NH_4 \cdot HF_2$ ensures a fluoride rich atmosphere in a covered crucible [9 - 11]. For melting of the glasses in *series I*, 5 mass % of $NH_4 \cdot HF_2$ was added to the batch. In *series II* (5 mass %) and *series IV* (0.5 mass %) NH_4F was added as fluorinating agent, while none was added to the batches of *series III*. Throughout this paper, we refer to

the various NAPF glasses by the mol % content of the added AlF_3. For example (100-x)$NaPO_3$-xAlF_3 with x = 10 is named NAPF-10.

All variations of the raw materials, crucibles and melting temperatures for the four glass series are listed in Table 1. The fluoride containing glasses were prepared in platinum crucibles for *series I, II* and *III*. Only *series IV* was melted in alumina crucibles.

All glasses of *series I* and *II* were melted in a 3-step process: 30 min at 400°C, 30 min at 800°C, and 15 min at 850°C. Care was taken not to exceed melting temperatures of 850°C at which P-F bonds become unstable and decompose [12 - 16]. During melting of NAPF-X glasses of *series III* and *IV* the melting temperatures were raised to 1000°C. Please refer to Table 1.

Table 1 for a systematic listing of the preparation parameter and temperatures.

For *series I* and *III* the melts were poured into preheated graphite moulds, for *series II* in non-preheated moulds, before annealing at T_g+50 K with a cooling rate of 3 - 5 K/min. For *series III* the glass samples were held for 4 hours at T_g +50K before cooling. The glasses of *series IV* were cast into pre-heated stainless steel moulds, kept at 450°C for about 1 h, and cooled to room temperature with a rate of about 3 K/ min.

Quantitative analysis

The fluorine content of the glass samples of *series I* was analyzed by wet chemical analysis after Ehrlich and Pietzka with a precision of ± 0.01 mass % [17]. An exact quantity of powdered glass samples is mixed with SiO_2 powder and boiled in H_3PO_4. The evaporating SiF_6 is collected in a NaOH solution where the fluorine dissolves, and is subsequently precipitated as PbBrF. Addition of $AgNO_3$ transforms PbBrF into AgBr, which can be titrimetically quantified through re-titration of $Na_2S_2O_3$ against SCN^-. The highest deviation from the theoretical fluorine content is found to be less than 15 % for the glass with only 20 mol % AlF_3, with lower relative fluorine loss for AlF_3 rich glasses (see Table 2).

For *series II* and *IV*, SEM-EDX was used for

Table 1. Comparison of the different preparation conditions of $NaPO_3$ and NAPF-X glasses for the four different glass series.

	Raw materials	batch	crucible	F-agent	melting	annealing	REF
$NaPO_3$ glass							
I	$NaPO_3$	100 g	SiO_2	-	800°C, 60 min	I-III	[7]
II	Na_2CO_3, $(NH_4)_2HPO_4$	50 g	Al_2O_3	-	30 min heating, 60 min at 790 °C	T_g+50K, 3-5 K/min	
III	$NaPO_3$	100 g	SiO_2	-	800 °C, 90 min		[8]
IV	$NaPO_3$	10 g	Al_2O_3	-	1000 °C, 60 min	450°C 60 min	
NAPF-X (X=10, 20, 30, 40)							
I	$NaPO_3$, AlF_3	100 g	Pt / lid	$NH_4{\cdot}HF_2$	850 °C[a]	I-III	[7]
II	v-$NaPO_3$, AlF_3	20 g	Pt / lid	NH_4H	850 °C[a]	T_g+50K,	
III	$NaPO_3$, AlF_3	100 g	Pt /lid	none	850-1000°C[b]	3-5 K/min	[8]
IV	$NaPO_3$, AlF_3	10 g	Al_2O_3 / no lid	NH_4H	1000-1100°C[c]	450°C 60 min	

[a] *3 step melting: 30 min at 400°C, 30 min at 800°C and 15 min at 850°C;*

[b] *60 min at 800°C and the last 30 minutes: NAPF10: 850°C; NAPF20: 900°C; NAPF30 and NAPF40: 1000°C (splat quenched to avoid crystallization);*

[c] *increasing times and temperatures for increasing AlF_3 content: NAPF10: 1100 °C (35 min); NAPF20: 1150°C (40 min);*

Table 2. Selected properties for $NaPO_3$ and NAPF-X glasses.

	F-retained, mass % [a,b]	T_g, °C (CTE, ppm/K)	Density, g/cm^3	REF	*More data to Series I* [7]
$NaPO_3$					
I	-	260 (24.5)	2.52	[7]	*n_e 1.4858*
II	-	263	2.49		*ν_e 65*
III	-	289	2.50	[8]	*900 ppmw OH*
IV	-	292	2.48		
NAPF-10					
I	*no sample*				
II	48%[a]	300	2.54		
III	***>95%*** [a]	311	2.55	[8]	
IV	<d.l. [a]	400	2.61		
NAPF-20					
I	86.2% [b]	305 (21.5)	2.63	[7]	*n_e 1.4722*
II	64% [a]	344	2.60		*ν_e 71*
III	***>95%*** [a]	325	2.62	[8]	*84 ppmw OH*
IV	10 % [a]	420	2.64		
NAPF-30					
I	88.1% [b]	335 (19.0)	2.71	[7]	*n_e 1.4689*
II	55% [a]	381	2.64		*ν_e 73*
III	***>95%*** [a]	367	2.68	[8]	*9 ppmw OH*
IV	*no sample*				
NAPF-40					
I*	99.6% [b]	405 (n.a.)	n.a. cr*	[7]	*n_e 1.4344*
II*#	70% [a]	421	2.75		*ν_e 80*
III	***>95%*** [a]	412	2.75	[8]	*OH n.a.*
IV	*no sample*				

n.a.: not analysed; - : not applicable; <d.l.: lower than the detection limit

[a] by SEM-EDX (large error margins, not yet optimized calibration);

[b] by wet chemical analysis, error < ± 0.01 mass %

** contains few $AlPO_4$ crystals, # contains some unreacted AlF_3*

quantitative analysis. While this method does not determine F and Al with high accuracy, it does provide relative good information on the P, O and Na content. It should be noted that the high quality of wet chemical analysis was based on an optimized set-up and ultimate practice of G. Heidemann, a now retired technician, and is not available to us anymore. We are aware that the error margins of SEM-EDX measurements are huge and we are currently in the process of improving the reliability by using various reference materials, including single crystals or chemically stable FP glasses. For glass *series III* a fluoride loss of less than 5 mass % is stated in reference [8] using SEM-EDX; however, no details were given regarding reference materials or the dependence on the nominal fluoride content. As Ehrt showed earlier for alkaline earth fluoride phosphate glasses [2, 18, 19] and as depicted in Fig. 1, the F-loss depends highly on the total fluoride content of the glasses. The more fluoride any FP glass contains initially, the lower the relative F-loss becomes. Therefore, a significant F-loss is expected to occur for the phosphate-rich and fluoride-poor NAPF samples, as confirmed by the analysis of the four glass *series I*, *II* and *IV* (see Table 2).

Physical Properties

Density

The density ρ of all glasses for all series was determined by the method of Archimedes, using various immersion liquids such as CCl_4 (at 25°C) with a precision of ± 0.001g/cm^3 for *series I*; or ethanol for *series II to IV* with a precision of ± 0.001- 0.01 g/cm^3 (at 21.1°C; *II, IV*) and ± 0.002 g/cm^3 (at 25°C, s*eries III*), respectively.

Glass transition temperature

For glasses of *series I*, the glass transition temperature T_g, as well as the coefficient of thermal expansion (*CTE*) were determined with a heating rate of 5 K/min by dilatometry.

For *series II* to *IV*, T_g was determined by differential scanning calorimetry (DSC, Netzsch) always using the onset method, the heating rate being 10 K/min for *series II+IV* and 20 K/min for s*eries III*.

Optical properties and refractive index

The refractive indices (n_e) in the visible range and the dispersion coefficient (v_e) were determined for all samples of *series I* with a Pulfrich refractometer (Δn ± 2 x 10^{-5}). The water content was deduced from the UV-Vis-NIR absorption spectra, which were recorded of polished plates from 3200 to 200 nm with a commercial spectrometer (SHIMADZU), and an error less than 1%.

Solid-state NMR spectroscopy

All reported spectra were obtained on a Bruker Avance Neo spectrometer with a magnetic flux density of 14.1 T and a commercial 2.5 mm triple resonance magic angle spinning (MAS) probe. ^{27}Al MAS NMR experiments were performed at a carrier frequency of 156.44 MHz using pulses with a small 30° flip angle of 1.0 µs duration, recycle delays of 0.25 s and sample spinning rates of 15 kHz. Chemical shifts are given relative to solid AlF_3 whose centre line shift was measured at -16.05 ppm in respect to a 1M aqueous solution of $Al(NO_3)_3$. Experimental data were analysed with the DMFIT software package [20], and the asymmetrically broadened central lines were fitted according to the Czjzek model.

Raman Spectroscopy

Raman spectroscopy measurements for *series II* were taken in backscattering geometry on unpolished glass samples using a HORIBA LabRAM HR800 Evolution spectrometer. Spectra were collected over the range of 10 - 1700 cm^{-1} using a 600 lines/mm grating and the 532 nm line of a diode laser. The spectral resolution is ~1.5 cm^{-1} while the 50 x objective yields a spatial resolution better than 2 µm.

The original Raman spectra of *series I* were collected in the range from 50 to 1500 cm^{-1} on a Jobin-Yvon spectrometer (Ramanor HG2S), with 5 cm^{-1} resolution and a 90° scattering geometry, using the 488 nm line of an Argon ion laser for excitation [4 - 6, 21]. An inVia Renishaw Raman microscope was employed for series III in the spectral range of 50 - 1500 cm^{-1}, using an excitation wavelength of 514.5 nm in a 90° scattering geometry [8]. All Raman spectra of Fig. 3 were normalized to the maximal intensity.

RESULTS AND DISCUSSION

Quantitative analysis

SEM-EDX was used to check the actual composition of the glasses of *series II* and *IV*, especially in regard to the loss of the volatile element fluorine. Generally, the analysed and nominal compositions agree well for Na, P and O (within 5 - 10 mass %), while Al is often significantly over-represented in the SEM-EDX analysis (up to 200 %, even in samples melted in Pt crucibles). Only the fluorine content is consistently lower than the nominal expected F-values, even though the F-content of CaF_2 single crystals or AlF_3 raw materials is close to the expected values. The quantitatively determined F-values are listed in Table 2.

More reliable than SEM-EDX are the wet chemical quantifications of the fluoride content of *series I*. In accordance with earlier findings by Ehrt [2, 18], the relative amount of retained fluoride increases for fluoride rich glasses, e.g. from 86.2 % F in NAPF-20 to 99.6 % F in NAPF-40 of *series 1*. Fig. 1 shows the dependence of fluoride retention on the total nominal fluoride content for various multicomponent fluoride phosphate glasses melted under air from the raw materials. It should be noted that the melting temperatures of these multicomponent glasses, which contain mostly divalent modifier cations, are much higher than the melting temperatures of the NAPF glasses of this study.

Comparison of the F-analysis data (Table 2) shows that melting at low temperatures, with $NH_4{\cdot}HF_2$ as fluorinating agent keeps fluoride retention high (*series I*), whereas most fluoride is lost from the phosphate

Table 3. Isotropic chemical shifts (δ_{CS}^{iso}), average quadrupolar coupling constants (CQ) and area fractions obtained from simulation of the ^{27}Al MAS NMR spectra using the Czjzek model for NAPF-10 and NAPF-20 glasses of series IV and II.

	Al species	δ_{CS}^{iso} / ppm ± 0.5 ppm	Average C_Q / MHz ± 0.1 MHz	Area fraction / % ± 1%
NAPF-10	Al^4	53.1	5.5	2
IV	Al^5	18.7	5.5	4
	Al^6	-6.3	5.1	94
NAPF-20	Al^4	45.7	4.0	1
IV	Al^5	18.8	5.7	6
	Al^6	−4.8	5.3	93
NAPF-20	Al^5	17.5	5.7	3
II	Al^6	−4.8	5.3	97

rich melts of *series IV* which were melted in alumina crucibles without a lid and with only trace additions of NH_4F (0.5 mass %). Also, the use of alumina crucibles in *series IV* leads to Al levels that, are increased by 50 % (NAPF-20) and even 100 % (NAPF-10) compared to Pt-crucible melted NAPF-20 and NAPF-10 glasses of *series II*. In *series IV,* only the glass NAPF-20 retains a fraction of 10 mass % F which is sufficient to exceed the detection limit in the SEM-EDX set-up used in this study. Note that for two NAPF glasses of *series IV* with comparable AlF_3 content of x = 15 mol % AlF_3, not discussed in the present study, SEM-EDX data indicates no detectable F retention. The F losses (as HF) can be formulated by the following reaction scheme for P rich glasses [12 - 16]:

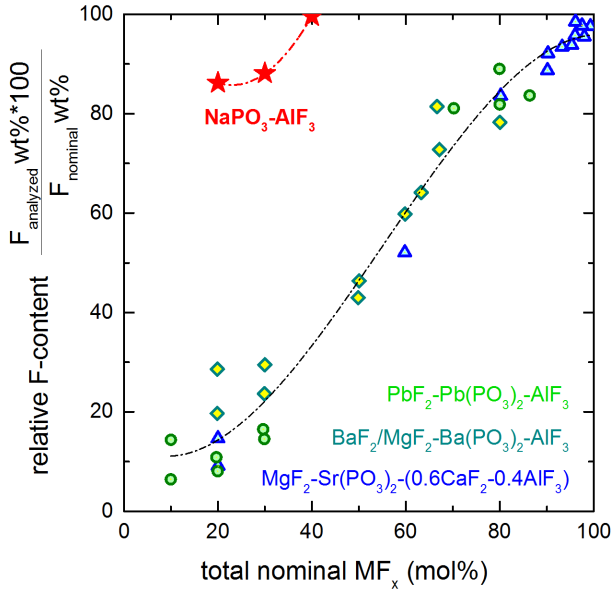

Fig. 1. Relative fluorine content in fluoride-phosphate glasses melted from different raw materials under air. The NAPF glasses of *series I* were melted at 800-850°C, the alkali free fluoride-phosphate glasses at 1100-1300°C (after Ehrt [2, 18, 19, 37]).

$$2 \equiv P-O-H \ + \ 2\,F-Al \equiv \xrightarrow{T} 2HF\uparrow + \\ +2 \equiv P-O-Al \equiv \qquad \text{Equation (1)}$$

Equation (1) depends hugely on the water content of the raw materials used, that is, on the H_2O and -OH content of AlF_3 or $NaPO_3$. Fluoride loss can also occur according to the reaction scheme depicted in equation (2) [12 - 16]:

$$3PFOO_{2/2} \quad (Q^2) \xrightarrow{T} POF_3\uparrow + 2PO_{3/2}O \quad (Q^3)$$

Equation (2)

^{27}Al MAS NMR

The ^{27}Al MAS NMR spectra of the *series IV* NAPF-10 glass and the two NAPF-20 glasses of *series IV* and *II,* see Fig. 2, show characteristic asymmetrically broadened resonance lines with isotropic chemical shifts around 18.8 ppm and -5.5 ppm corresponding to five- and six-

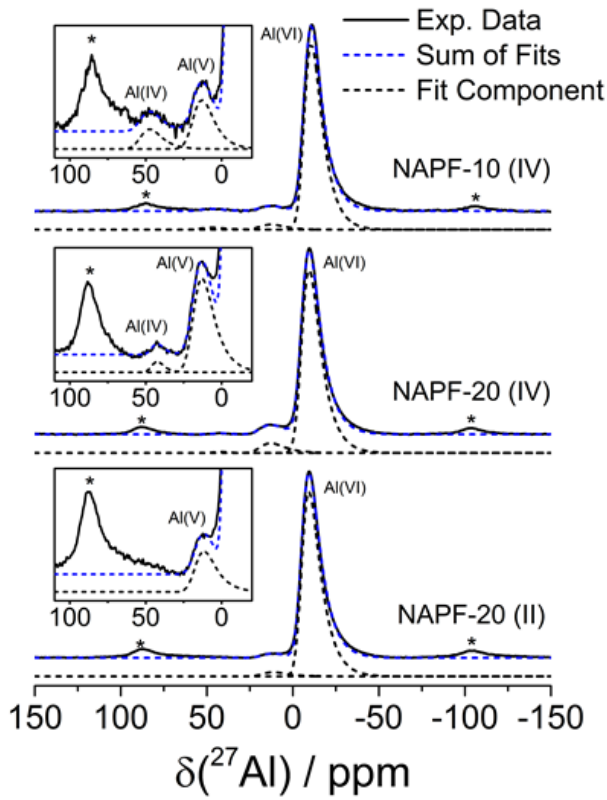

Fig. 2. ^{27}Al MAS NMR spectra of NAPF-10 glass of *series IV* and NAPF-20 glasses of *series IV* and *II*. The sum of the simulated spectra (dashed lines) is superimposed on the experimental data and spinning sidebands are marked with an asterisk. Vertical expansions showing low concentrations of Al(IV) and Al(V) are included.

coordinated Al. The glasses of *series IV* additionally feature very small amounts of Al(IV) at isotropic chemical shift values of around 49.4 ppm. ^{27}Al is a quadrupole nucleus with spin quantum number I = $^5/_2$ and thus line shapes are affected by second order quadrupole perturbations in the presence of an electric field gradient distribution. In order to retrieve meaningful information, the recorded spectra were thus deconvoluted by the Czjzek model, assuming a statistical distribution of quadrupole parameters η_Q (asymmetry factor) and CQ (quadrupole coupling constant). The good agreement achieved between spectra and deconvolution, reflects thus the high degree of disorder in the glassy samples, see Table 3.

While absolute aluminum concentrations are not readily available from MAS NMR, it is quite remarkable that, despite the relatively low F content and high Al intake for NAPF-10 and NAPF-20 samples molten in alumina crucibles (*series IV*), the preferred coordination state remains almost exclusively sixfold as in the NAPF-20 glass molten in a Pt crucible.

Overall, the obtained values of δ_{CS}^{iso} and average CQ for all Al-species show only very little variation amongst the individual samples. The significant difference between the Al(IV) resonances observed in NAPF-20 and NAPF-10 are to be considered with caution, as they probably arise from the comparably high errors of deconvoluting signals of such low intensity. Further, ^{27}Al{^{19}F} double resonance experiments, in which both nuclei's dipolar interaction can be probed and which could principally yield information about the ratio of O and F in the Al(O,F)$_6$ octahedra, were not conducted for glasses of *series IV*. The average ^{27}Al - ^{19}F distances are expected to be rather high, and the effectiveness of the experiment is insufficient in the present regime of low AlF_3 concentrations.

Contrary to fluoride-containing glasses, where Al-NMR could only detect sixfold coordinated Al-ions, five- and four-fold coordinated Al - ions are commonly found in oxide phosphate glasses [2, 6, 18, 22 - 26].

Raman spectroscopy

Fig. 3 shows the Raman spectra of the four NAPF glass series. The spectra of pure $NaPO_3$-glasses are depicted in Fig. 3a, while Figs. 3b to 3e display the spectra of (100 - x)$NaPO_3$-xAlF_3 glasses with increasing AlF_3-content (x = 10 to 40 mol %).

No significant variations are observed for the pure metaphosphate glass between the four series (Fig. 3a). The main bands at 685 cm^{-1} and 1165 cm^{-1} are typical for the symmetric stretching modes of P-O-P bridges between metaphosphate tetrahedra, ν_s(P-O-P), and the symmetric stretching modes of P-O$^-$ bonds, $\nu_s(PO_2^-)$, of these metaphosphate tetrahedra, respectively [4, 21, 27]. In the following, the Q^n nomenclature is used to state the number of *n* bridging (and consequently *4-n* terminal) oxygen atoms per phosphate tetrahedron. Metaphosphate tetrahedra are thus labelled as Q^2 groups. Bending modes of phosphate groups also contribute at low energies, in the 300 to 425 cm^{-1} range [9, 21, 27 - 34]. Some disproportionation of Q^2 groups into Q^1 and Q^3 groups accounts for the additional low intensity bands at ca. 1015 cm^{-1} and 1310 cm^{-1}, respectively, while the asymmetric stretching mode of Q^2 groups is also evident at ca. 1265 cm^{-1} [21, 27 - 29, 35].

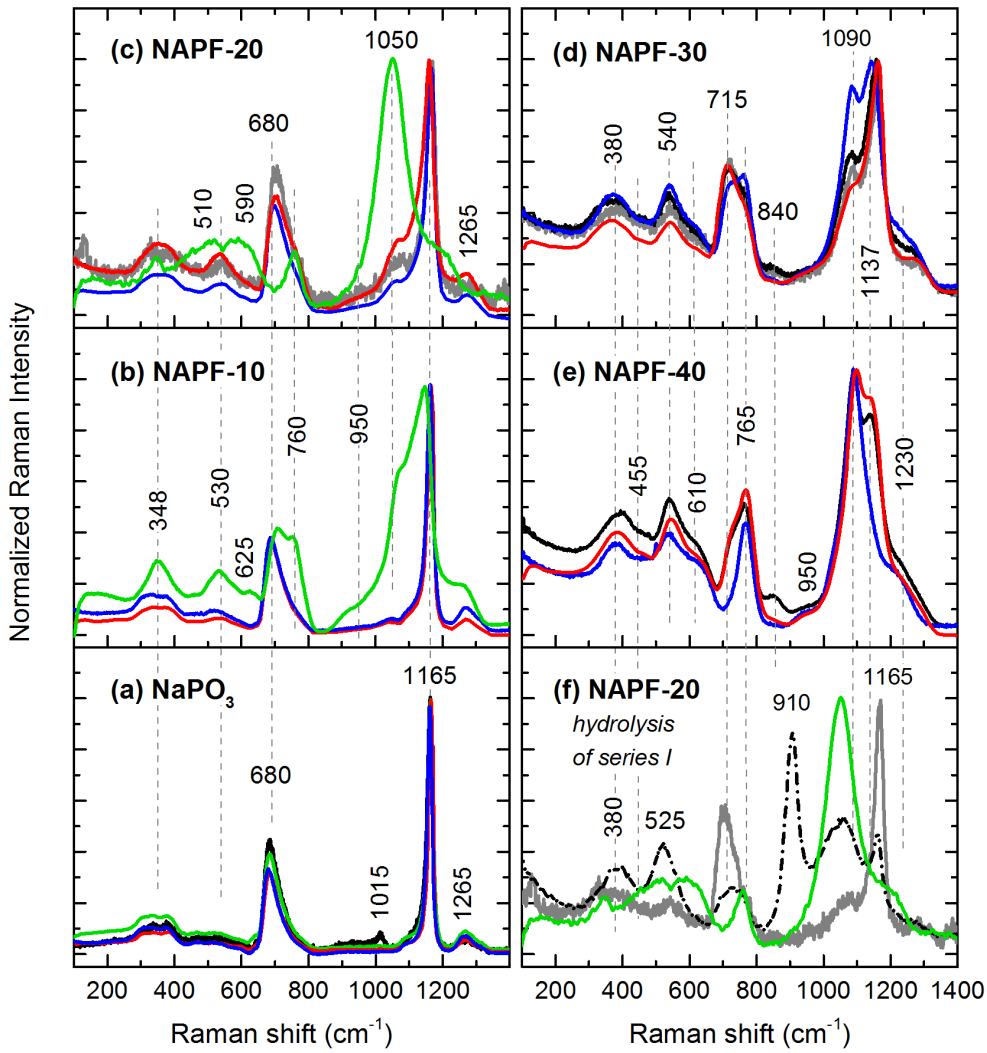

Fig. 3. Raman spectra of the four series of NAPF glasses. *Series I*: black for spectra obtained in 2016 and grey for spectra obtained 2006; *Series II*: blue; *Series III:* red ; *Series IV:* green. The bottom right figure (f) is included to show the effect of hydrolysis of the P-rich sample NAPF-20 of *series I* (broken line) compared to *I* and *IV* from (c) and to facilitate comparison of the spectra in the NAPF series of the left and right column.

The Raman spectra of glasses from *series I* to *III* are quite similar for low AlF_3 contents, such as x = 10 (Fig. 3b) or x = 20 (Fig. 3c). Here, only the glasses from *series IV*, which were melted in alumina crucibles without lids, contrast significantly. For a comparison amongst glasses with high AlF_3 content only samples of *series I* through *III* are available, i.e. x = 30 (Fig. 3d) and x = 40 (Fig. 3e). For those glasses, we see significant differences depending on the fluorinating agent used (NH_4HF_2 for *series I* or NH_4F for *series II*), but also for the various melting temperatures which did not exceed 850°C in *series I* and *II*, but increased up to 1000°C in *series III*.

Glasses of *series IV* show clearly the role of Al_2O_3 leached from the crucible on the depolymerization of the metaphosphate glass network. We also note significant band shifts, as the high field strength Al^{3+} ions are increasingly substituted for the monovalent Na^+ ions as the charge balancing cations and as cross-linker. Before discussing the effect of AlF_3 addition for *series I*, *II* and *III*, we want to focus first on *series IV*, where SEM-EDS showed that most of the fluorine was lost. A listing of the Raman assignments can be found in Table 4.

Table 4. Assignments of Raman bands.

Raman shift (cm^{-1})	
$NaPO_3$	[21, 30, 36]
300-400 w	$\delta(PO_2^-)$ Q^2
680 m	ν_s(P-O-P) Q^2
1015w	$\nu_s(PO_3^{2-})$ Q^1
1165 vs	$\nu_s(PO_2^-)$ Q^2
1265 w	$\nu_{as}(PO_2^-)$ Q^2
1320 vw	ν_s(P=O) Q^3
NAPF-20-IV (F-free)	[27, 32, 34]
348 w	$\delta(PO_3^{2-})$ Q^1
	$\nu_2(PO_4^{3-})$ Q^0
440-520 m	Al-O-P
565-620 m	$\nu_4(PO_4^{3-})$ Q^0
	Al-O-P
760 m	ν_s(P-O-P) Q^1
	Al-O-P
950 m	$\nu_4(PO_4^{3-})$ Q^0
1050 vs, b	$\nu_s(PO_3^{2-})$ Q^1
1180 m	$\nu_s(PO_2^-)$ Q^2
Hydrolysed NAPF-20	[27, 28, 31-34]
380 w, b	$\delta(PO_3^{2-})$ Q^1
	$\nu_2(PO_4^3)$ Q^0
525 m	$\nu_4(PO_4^{3-})$ Q^0
730 w	ν_s(P-O-P) Q^1
910 vs	ν_s(P-OH)
1055 s	$\nu_s(PO_3^{2-})$ Q^1 (Al^{3+})
1163 m	$\nu_s(PO_2^-)$ Q^2
1240 vw	$\nu_{as}(PO_2^-)$ Q^2
NAPF-40-I	[4-6]
400 w	nw deformation
455 w	O-P bending
540 w	Al-F/O in $Al(O,F)_6$
610 m	$\nu_4(PO_4^{3-})$ Q^0
715 m	ν_s(P-O-P) Q^2
	(short chains?)
765 m	ν_s(P-O-P) Q^1
	Al-O-P
840 w	P-F
950 w	$\nu_4(PO_4^{3-})$ Q^0
1090 vs	$\nu_s(PO_3^{2-})$ Q^1 (Al^{3+})
1137 s	$\nu_s(PO_2^-)$ Q^2
1230 w	$\nu_{as}(PO_2^-)$ Q^2

Series IV

As shown in Table 2, only the glass NAPF-20 retained 10 % of total fluorine, while the F-levels were below the detection level for NAPF-10 of *series IV*. As fluoride was lost from the melt, oxygen uptake from the atmosphere accounts for anion and charge balance. However, the number of Al^{3+} ions is much higher than expected from the nominal composition because dissolved Al_2O_3 from the crucibles adds to the total modifier oxide content of the melt [31, 33].

The Raman spectra of *series IV* (Figs. 3b, c) show the evolution of bands at 760 and 1050 cm^{-1}. For NAPF-10, these bands appear as shoulders to the stretching modes of ν_s(P-O-P) at 685 cm^{-1} and $\nu_s(PO_2^-)$ at 1165 cm^{-1}. These bands shift to higher and lower energies, respectively, as the phosphate network is progressively depolymerized. For x = 20, these new bands at 760 and 1050 cm^{-1} are dominant in the Raman spectrum. The 760 cm^{-1} band can be assigned to P-O-P bridges connecting two Q^1 groups (pyrophosphate $P_2O_7^{4-}$) and the 1050 cm^{-1} band to the corresponding $\nu_s(PO_3^{2-})$ stretching mode [27, 28, 33]. The low intensity of the 760 cm^{-1} band, compared to the analogous stretching mode between Q^2 units, as evidenced for the glasses of *series I* to *III* at 710 cm^{-1}, reflects the high degree of depolymerization in the glass of *series IV*. As shown in many other previous studies, the depolymerization of the phosphate network shifts the $P\text{-}O^-$ stretching modes to lower energies, while the substitution of a large or low charge cation such as Na^+ by a smaller cation of higher valence, such as Al^{3+}, will shift the position of the $P\text{-}O^-$ stretching mode to higher energies [21, 33, 36]. Weak bands around 515 and 550 - 650 cm^{-1} can be assigned to O-P-O bending modes, as well as to vibrations of P-O-Al bonds. The bands around 500 cm^{-1} are absent from any other spectra and might therefore arise from mixed bending modes of phosphate and aluminate polyhedra as well as from Al-O-Al bridges. The Raman spectrum of NAPF-20 (*series IV*) compares well as a whole with other alumo-pyrophosphate type glasses, such as the $40Na_2O$-$19Al_2O_3$-$39P_2O_5$-$2B_2O_3$ mol % samples reported by Grigg et al. [26] and the xAl_2O_3 – (1-x) $NaPO_3$ glass series reported by Brow et al for x = 0.13 [27]. It is interesting to note that the Al-coordination determined by ^{27}Al-NMR for the glass with x=0.13 is dominated by AlO_6, with only minor contribution of AlO_5 and AlO_4, in agreement with our NMR data of the glasses in *series IV*. Conversely, Brow et al found for x = 0.26 a shift to predominantly lower coordinated Al-species and in the Raman spectrum the absence of any P-O-P bridges [27].

Series I to III

Compared to *series IV*, the observed changes in the Raman spectra of the x = 10 and x = 20 glasses in *series*

I, *II* and *III* are much smaller, as the metaphosphate backbone remains the dominant structural characteristic. Small changes at 1065 and 760 cm^{-1} are indicative for a beginning depolymerization of the metaphosphate structures. These changes become more pronounced for x = 30 and x = 40, with the main $P\text{-}O^-$ stretching mode shifting to lower energies. The shift is less pronounced than it would be for a pure sodium-phosphate glass, as the high field strength Al^{3+} ion is contributing now as a charge balancing cation and, consequently, raises the energy of the $P\text{-}O^-$ stretching modes. Close to the stretching modes $\nu_s(PO_3^{2-})$ of Q^1 groups around 1015 cm^{-1} emerges a weak shoulder around 950 cm^{-1}, which may correspond to the stretching modes $\nu_s(PO_4^{3-})$ of orthophosphate Q^0 groups [32, 34].

Other features like the shoulder at 620 cm^{-1} resembles the observations already discussed for *series IV*, reflecting the increased depolymerization of the phosphate network and increasing formation of Al-O-P bridges. The possible assignment of this shoulder to AlF_4 tetrahedra as proposed in ref. [8] should be excluded on the basis of our NMR data on NAPF-20 (*series II*) and the more extensive data of *series I* reported in ref. [6, 7], which gave no evidence of any significant tetrahedral aluminate fraction in glasses of the NAPF series.

General agreement is found for most other Raman assignments involving fluoride bonds, such as the vibrations of sixfold coordinated Al^{3+} with a mixed oxide and fluoride environment, $Al(F,O)_6$, giving rise to the band around 540 cm^{-1} [4 - 6, 8]. Furthermore, the weak feature at 850 cm^{-1} can be assigned to the stretching of fluorophosphate bonds, P-F. While this feature is only hinted at in the glasses of *series II to IV*, it appears as a well-separated and distinct band in glasses x = 30 and x = 40 of *series I*. This observation confirms earlier studies by Ehrt et al. concerning the instability of P-F bonds above 850°C [12 - 16] and unpublished data, including the Dissertation Thesis of Frank Möwius [Akademie der Wissenschaften, Berlin, Germany, 1975]. Only traces of P-F bonds are evident in the F-rich glasses of *series II* and *III*, and possibly also in all glasses with x = 20, even those of *series IV*. Even though *series II* was melted at equally low temperatures, the use of a suboptimal fluorinating agent is probably the reason for the higher oxygen uptake and the low number of P-F bonds formed.

The relative intensities of the stretching modes associated with Q^2 groups (1135 and 715 cm^{-1}) and of chain ending Q^1 groups (1090 cm^{-1} and 770 cm^{-1}) reflect the degree of depolymerization of the various glasses. The difference in band positions of Q^1 units in glasses of *series I* to *III* and *series IV* are probably two-fold. *Series IV* contains predominantly orthophosphate (Q^0) and pyrophosphate ($P_2O_7^{4-}$ groups), whereas the glasses of *series I* to *III* contain metaphosphate (Q^2) and chain ending Q^1 groups. The position of $P\text{-}O^-$ stretching modes of chain ending Q^1 groups can be found at lower energies than of two linked Q^1 groups in a pyrophosphate unit [33]. On the other hand, the 1050 cm^{-1} band of *series IV* is very broad, and deconvolution might have to consider Al-O-P bonds, as well as stretching modes of Q^0 and Q^1 units. Evidently, oxygen uptake is much higher for glasses without or with NH_4F instead of $NH_4{\cdot}HF_2$ addition as in *series I*. The higher degree of polymerization observed for *series III* might in turn be explained by the evaporation reaction of equation (2), by the loss of volatile POF_3 at higher temperatures.

NAPF-40 is generally prone to crystallization, and was therefore splat quenched in *series III*. The bulk NAPF-40 sample of *series I* contains few visible inclusion of $AlPO_4$ crystals (see Fig. 5) [12 - 16, 37].

Earlier studies showed the formation of Na_3AlF_6 crystals upon crystallization experiments of fluoride phosphate glasses, and thus confirmed the analogous structure of octahedral fluoro-aluminate units in fluoride phosphate glasses [12 - 16, 37].

Structure-property correlation

Insertion of $Al(O,F)_6$ octahedra into the metaphosphate chains densifies the network and counterbalances the lower mass of AlF_3 compared to $NaPO_3$. The density was found to increase in all four glass series similarly as the nominal AlF_3 content increases (see Fig. 4a). This is not surprising if one considers the similar masses of $NaPO_3$ (102 g/mol), AlF_3 (84 g/mol) and Al_2O_3 (102 g/mol). The higher density of the x = 10 sample of *series IV* compared to the fluorinated counterparts of *series II* and *III* can be explained by the additional uptake of significant amounts of Al_2O_3 from the crucible material.

T_g-values increase pronouncedly with increasing nominal AlF_3 levels (Fig. 4b), while the coefficient of thermal expansion CTE (available only for *series I*) decreases with the addition of AlF_3. In Fig. 4b we also see huge differences in the experimental T_g values, which can be attributed only partially to different methods of

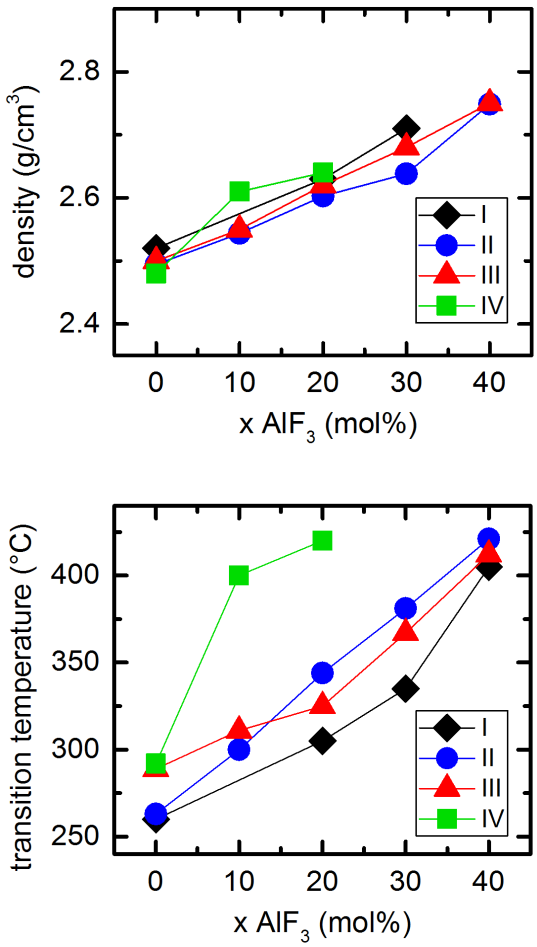

Fig. 4. a) Variation in density of the four series of (100-x) $NaPO_{3-x}AlF_3$ glasses with increasing AlF_3 content, b) Variation in the transition temperature, T_g, of the four series of (100-x)$NaPO_{3-x}AlF_3$ glasses with increasing AlF_3 content.

measurements (dilatometry for *series I*, DSC with a heating rate of 20 K/min in *series III* and a rate of 10 K/min in *series II* and *IV*). Apparently fluoride loss and simultaneous Al_2O_3 uptake, as for *series IV*, increase the T_g most prominently. This effect has been discussed in detail for silver phosphate [31, 33] or tellurite glasses [38]. The relative high T_g value for NAPF-10 of *series III* might be explained by an increased F-evaporation and subsequent oxygen uptake for the P rich glasses [8]. The differences in T_g for the pure metaphosphate glasses are unclear, since *series II* and *IV* were melted in Al_2O_3 crucibles and measured with the same DSC set up and heating rate while both *series I* and *III* were prepared

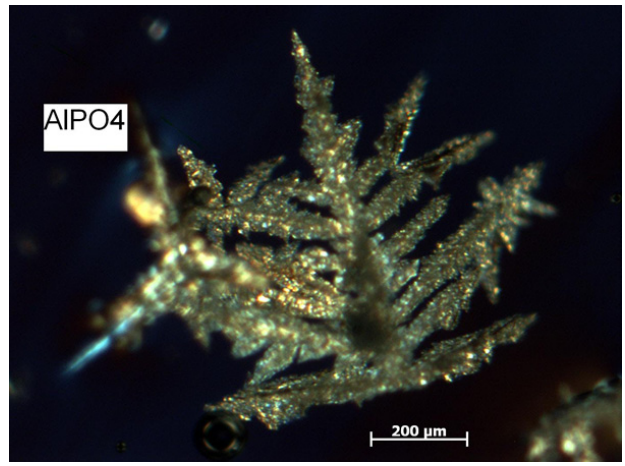

Fig. 5. $AlPO_4$ crystal in NAPF-40 (*series I*), photograph taken on a plane parallel polished glass sample (thickness 2 mm), with a polarizing microscope (CARL ZEISS Jena) with crossed Nicols. $AlPO_4$ has small birefringence (Δn).

in SiO_2 crucibles. However, both *series III* and *IV* were melted 30 minutes longer than *series I* and *III*, which might have enhanced crucible material uptake in *series IV* while minimizing the water content of these glasses.

From the O-H vibration in the near IR (3200 nm) the OH-content was determined for the glasses of *series I* [39]. The highest water content was found for the $NaPO_3$ glass with (E/d) 3100 nm = 30 cm^{-1}, or around 900 ppmw OH. The water content decreases drastically with the introduction of AlF_3 to 2.8 cm^{-1} ≈ 84 ppmw (x = 20) and 0.3 cm^{-1} ≈ 9 ppmw (x = 30). The loss of water, or better hydrogen from the glass, follows the reaction scheme shown in equation (1). The corresponding increase in chemical stability of glasses containing high AlF_3 contents is evident, as for instance, the NAPF-20 glass made in 2006 displays today a partially corroded surface (see also the Raman evidence in Fig. 4f), while NAPF-30 and NAPF-40 show no such deterioration after a decade in storage.

More detailed optical properties are currently available only for glasses of *series I* (see Table 2). Optical absorption spectroscopy showed for 1 cm thick glasses of *series I* a high transparency, with the UV absorption edge below 200 nm. Also, the n_e-values decrease and the ν_e-values increase with the addition of AlF_3. As the refractive index depends directly on the average anion polarizability of the glass, and fluoride has a much lower polarizability than oxygen, small variations in the O:F content are readily observable in variations of the refractive index [40 - 42].

CONCLUSIONS

Variations in the preparation methods (raw materials, fluorinating agents, crucible and melting temperatures) have a significant impact on the composition, structure and, subsequently, the properties of fluoroaluminate-phosphate-glasses.

Of the four nominally identical series of the NAPF glass composition (100-x)$NaPO_3$-xAlF_3 with x = 0 to 40 mol %, series (*IV*) resembles more a (100-x) $NaPO_3$-xAl_2O_3 glass, since these glasses were melted in alumina crucibles without a lid. This resulted in almost complete fluoride by oxygen substitution and addition of Al_2O_3 to the glass by dissolution of the alumina crucible. As a consequence, the phosphate network was more depolymerized (Q^0 and Q^1 for NAPF-20), but the phosphate entities are strongly cross-linked by Al^{3+} ions and, as a consequence, result in T_g values higher than those for the *series I* to *III* melted with a lid (see also [43]).

Addition of the fluorinating agent NH_4.HF_2 was crucial for keeping fluoride retention high. Furthermore, only for high fluorination and low melting temperatures (not exceeding 850°C) significant amounts of P-F bonds were found to form in the studied glasses (*series I*). Reactions with water present in the raw materials and in the melting atmosphere results in F-losses through formation of HF and substitution of fluoride in the glass network by oxide. Melting at too high temperatures also results in a higher polymerization of the phosphate network as POF_3 evaporates and Q^3 units form. For F-rich glasses, such as NAPF-40, $AlPO_4$ as well as Na_3AlF_6 crystals may form (see Fig. 5).

Ideally, when preparing NAPF glasses we recommend using lid-covered Pt crucibles with NH_4·HF_2 as a fluorinating agent, while not exceeding melting temperatures of 850°C in order to attain reproducible glass batches with consistent properties.

Acknowledgements

DM, BJAM and ACMR thank FAPESP (process number: 2017/029536 and 2013/07793-6) for financial support of this project. MCBN wants to acknowledge financial aid from CAPES and the Post-Graduate Program of Materials Science and Engineer (PPGCEM)/ UFSCar. BJAM would also like to thank Paulo Sergio Pizani for hosting his project and contributing with discussions, instrumental and related materials, as well as CNPq, CAPES, as well as FAPES (process no. 2016/18567-5) for funding. HB thanks FAPESP (grant no. 2013/07793-6 via the CEPID programme) for financial support and Hellmut Eckert at USP-IFSC, Sao Carlos, Brazil for the use of lab and NMR equipment. EIK acknowledge support by the project "Advanced Materials and Devices" (MIS 5002409) which is implemented under the "Action for the Strategic Development on the Research and Technological Sector", funded by the Operational Programme "Competitiveness, Entrepreneurship and Innovation" (NSRF 2014-2020) and co-financed by Greece and the European Union (European Regional Development Fund).

The help of Yoshi Fernando (LCE /DEMaUFSCar) in SEM-EDX measurements is gratefully acknowledged.

REFERENCES

1. D. Ehrt, Fluoroaluminate glasses for lasers and amplifiers, Current Opinion in Solid State & Materials Science, 7, 2003, 135-141, https://doi.org/10.1016/s1359-0286(03)00049-4
2. D. Ehrt, REVIEW Phosphate and fluoride-phosphate optical glasses - properties, structure and applications, Phys. Chem. Glasses: Eur. J. Glass Sci. Technol. B, 56, 2015, 217-234, https://doi.org/10.13036/17533562.56.6.217
3. M. de Oliveira, T.S. Gonçalves, C. Ferrari, C.J. Magon, P.S. Pizani, A.S.S. de Camargo, H. Eckert, Structure–property relations in fluorophosphate glasses: An integrated spectroscopic strategy, J. Phys. Chem. C, 121, 2017, 2968-2986, https://doi.org/10.1021/acs.jpcc.6b11405
4. D. Möncke, D. Ehrt, L.L. Velli, C.P.E. Varsamis, E.I. Kamitsos, Structural investigations of fluoride phosphate glasses, Proc. XX Int. Congr. Glass, P-10-030, 2004, 1-6.
5. D. Möncke, D. Ehrt, L.L. Velli, C.P.E. Varsamis, E.I. Kamitsos, Structure and properties of mixed phosphate and fluoride glasses, Phys. Chem. Glasses, 46, 2005, 67-71.
6. D. Möncke, D. Ehrt, L.L. Velli, C.P.E. Varsamis, E.I. Kamitsos, S. Elbers, H. Eckert, Comparative spectroscopic investigation of different types of fluoride phosphate glasses, Phys. Chem. Glasses: Eur. J. Glass Sci. Technol. B, 48, 2007, 399-402.
7. H. Bradtmüller, L. Zhang, C.C. de Araujo, H. Eckert,

D. Möncke, D. Ehrt, Structural studies of $NaPO_3$-AlF_3 glasses by high-resolution double-resonance NMR spectroscopy, in press, The Journal of Physical Chemistry C 2018.

8. Q.H. Le, T. Palenta, O. Benzine, K. Griebenow, R. Limbach, E.I. Kamitsos, L. Wondraczek, Formation, structure and properties of fluoro-sulfo-phosphate poly-anionic glasses, J. Non-Cryst. Solids, 477, 2017, 58-72, https://doi.org/10.1016/j.jnoncrysol.2017.09.043
9. R.K. Brow, Z.A. Osborne, R.J. Kirkpatrick, A multinuclear MAS NMR study of the short-range structure of fluorophosphate glass, J. Mater. Res., 7, 1992, 1892-1899, https://doi.org/10.1557/JMR.1992.1892
10. T. Djouama, A. Boutarfaia, M. Poulain, Fluorophosphate glasses containing manganese, J. Phys. Chem. Solids, 69, 2008, 2756-2763, https://doi.org/10.1016/J.Jpcs.2008.07.004
11. G. Galleani, S.H. Santagneli, Y. Messaddeq, M. de Oliveira, H. Eckert, Rare-earth doped fluoride phosphate glasses: structural foundations of their luminescence properties, PCCP, 19, 2017, 21612-21624, https://doi.org/10.1039/C7CP03927A
12. D. Ehrt, C. Jäger, Investigations of solid-state reactions of binary polyphosphate fluoride systems by means of thermal-analysis, X-ray diffractio and NMR spectroscopy. 2. Systems $Sr(PO_3)_2$+SrF_2 and $Ca(PO_3)_2$+CaF_2, Zeitschrift für Physikalische Chemie Neue Folge, 159, 1988, 89-102, https://doi.org/10.1524/zpch.1988.159.Part_1.089
13. C. Jäger, D. Ehrt, Investigations of solid-state reactions of binary polyphosphate fluoride systems by means of thermal-analysis, X-ray diffraction and NMR-spectroscopy. 3. System $Mg(PO_3)_2$+MgF_2, Zeitschrift für Physikalische Chemie Neue Folge, 159, 1988, 103-112, https://doi.org/10.1524/zpch.1988.159.Part_1.103
14. C. Jäger, D. Ehrt, U. Haubenreisser, Investigations of solid-state reactions of binary polyphosphate fluoride systems by means of thermal-analysis, X-ray diffraction and NMR-spectroscopy. 1. System $Ba(PO_3)_2$+BaF_2, Zeitschrift für Physikalische Chemie Neue Folge, 159, 1988, 75-87, https://doi.org/10.1524/zpch.1988.159.Part_1.075
15. D. Ehrt, C. Jäger, Investigations of solid-state reactions of binary polyphosphate fluoride systems by means of thermal-analysis, X-ray diffraction and NMR-spectroscopy. 6. Reactions of $Mg(PO_3)_2$, $Ba(PO_3)_2$ and $La(PO_3)_3$ with an excess of AlF_3, Zeitschrift für Physikalische Chemie Neue Folge, 165, 1989, 55-65. https://doi.org/10.1524/zpch.1989.165.Part_1.055
16. C. Jäger, D. Ehrt, Investigations of solid-state reactions of binary polyphosphate fluoride systems by means of thermal-analysis, X-ray diffraction and NMR-spectroscopy. 5. Reactions of $Sr(PO_3)_2$ with AlF_3, CaF_2 and MgF_2, Zeitschrift für Physikalische Chemie Neue Folge, 162, 1989, 109-118, https://doi.org/10.1524/zpch.1989.162.Part_1.109
17. P. Ehrlich, G. Pietzka, Die maßanalytische Bestimmung des Fluors nach Fällung als Bleibromofluorid, Fresenius Zeitschrift für analytische Chemie, 133, 1951, 84-94, https://doi.org/10.1007/bf00452244
18. D. Ehrt, Grundlagenuntersuchungen für die Entwicklung von Fluorophosphat- und Fluoroaluminatgläsern mit extremer positiver anomaler Teildispersion, in, Dissertation B (Dr. sc. nat), Friedrich-Schiller-University, Jena, 1984, (in German).
19. D. Ehrt, R. Atzrodt, W. Vogel, Struktur-Eigenschaftsbeziehungen optischer Gläser mit anomaler Teildispersion; 2. International Otto-Schott-Colloquium, Wissenschaftliche Zeitschrift der Friedrich-Schiller-University, Jena, Germany, 1982, pp. 509-526, (in German).
20. D. Massiot, F. Fayon, M. Capron, I. King, S. Le Calvé, B. Alonso, J.-O. Durand, B. Bujoli, Z. Gan, G. Hoatson, Modelling one- and two-dimensional solid-state NMR spectra, Magn. Reson. Chem., 40, 2002, 70-76, https://doi.org/10.1002/mrc.984
21. L.L. Velli, C.P.E. Varsamis, E.I. Kamitsos, D. Möncke, D. Ehrt, Structural investigation of meta-phosphate glasses, Phys. Chem. Glasses, 46, 2005, 178-181.
22. L. Zhang, C.C. de Araujo, H. Eckert, Aqueous sol-gel preparation of Na_2O - Al_2O_3 - B_2O_3 glasses: structural characterisation by liquid and solid state NMR spectroscopy, Phys. Chem. Glasses - Eur. J. Glass Sci. Technol. B, 47, 2006, 7-15.
23. L. Zhang, H. Eckert, Short- and medium-range order in sodium aluminophosphate glasses: New insights from high-resolution dipolar solid-state NMR spectroscopy, J. Phys. Chem. B, 110, 2006, 8946-8958, https://doi.org/10.1021/jp060501s
24. L. Zhang, C.C. de Araujo, H. Eckert, Structural role of fluoride in aluminophosphate sol−gel glasses: High-resolution double-resonance NMR studies, J.

Phys. Chem. B, 111, 2007, 10402-10412, https://doi.org/10.1021/jp072725w
25. L. Zhang, H. Eckert, Influence of phosphate precursors on the structures of sodium aluminophosphate sols, gels and glasses, J. Non-Cryst. Solids, 354, 2008, 1331-1337. http://dx.doi.org/10.1016/j.jnoncrysol.2006.10.089
26. A.T. Grigg, A.J. Marsden, M. Mee, S. Feller, S.K. Fong, P.M. Mallinson, R. Dupree, D. Holland, Vitrification of β-tricalcium phosphate in sodium aluminoborophosphate glass and the effect of Ga^{3+} substitution, J. Solid State Chem., 231, 2015, 175-184. https://doi.org/10.1016/j.jssc.2015.08.023
27. R.K. Brow, D.R. Tallant, Structural design of sealing glasses, J. Non-Cryst. Solids, 222, 1997, 396-406, http://dx.doi.org/10.1016/S0022-3093(97)90142-3
28. R.K. Brow, Review: the structure of simple phosphate glasses, J. Non-Cryst. Solids, 263-264, 2000, 1-28, http://dx.doi.org/10.1016/S0022-3093(99)00620-1
29. R.K. Brow, D.R. Tallant, J.J. Hudgens, S.W. Martin, A.D. Irwin, The short-range structure of sodium ultraphosphate glasses, J. Non-Cryst. Solids, 177, 1994, 221-228, http://dx.doi.org/10.1016/0022-3093(94)90534-7
30. R.K. Brow, D.R. Tallant, S.T. Myers, C.C. Phifer, The short-range structure of zinc polyphosphate glass, J. Non-Cryst. Solids, 191, 1995, 45-55, http://dx.doi.org/10.1016/0022-3093(95)00289-8
31. I. Konidakis, C.P.E. Varsamis, E.I. Kamitsos, Effect of synthesis method on the structure and properties of $AgPO_3$-based glasses, J. Non-Cryst. Solids, 357, 2011, 2684-2689, https://doi.org/10.1016/j.jnoncrysol.2011.03.013
32. D. Möncke, S. Sirotkin, E. Stavrou, E.I. Kamitsos, L. Wondraczek, Partitioning and structural role of Mn and Fe ions in ionic sulfophosphate glasses, J. Chem. Phys., 141, 2014, 224509, http://dx.doi.org/10.1063/1.4903191
33. D. Palles, I. Konidakis, C.P.E. Varsamis, E.I. Kamitsos, Vibrational spectroscopic and bond valence study of structure and bonding in Al_2O_3-containing AgI-$AgPO_3$ glasses, RSC Advances, 6, 2016, 16697-16710, https://doi.org/10.1039/C6RA00162A
34. A. Thieme, D. Möncke, R. Limbach, S. Fuhrmann, E.I. Kamitsos, L. Wondraczek, Structure and properties of alkali and silver sulfophosphate glasses, J. Non-Cryst. Solids, 410, 2015, 142-150, http://dx.doi.org/10.1016/j.jnoncrysol.2014.11.029
35. K. Meyer, Characterization of the structure of binary zinc ultraphosphate glasses by infrared and Raman spectroscopy, J. Non-Cryst. Solids, 209, 1997, 227-239, http://dx.doi.org/10.1016/S0022-3093(96)00563-7
36. B.N. Nelson, G.J. Exarhos, Vibrational spectroscopy of cation-site interactions in phosphate glasses, J. Chem. Phys., 71, 1979, 2739-2747, http://dx.doi.org/10.1063/1.438679
37. D. Ehrt, C. Jäger, W. Vogel, Reaktionsprozesse bei der Glasbildung und Rekristallisation von Fluoroaluminatgläser; International Otto-Schott Colloqium, Wiss. Zeitschr. Friedrich-Schiller-Univ. Jena, Naturwiss. R., Jena, Germany, 1987, pp. 867-884, (in German).
38. N.S. Tagiara, D. Palles, E.D. Simandiras, V. Psycharis, A. Kyritsis, E.I. Kamitsos, Synthesis, thermal and structural properties of pure TeO_2 glass and zinc-tellurite glasses, J. Non-Cryst. Solids, 457, 2017, 116-125, https://doi.org/10.1016/j.jnoncrysol.2016.11.033
39. H. Ebendorff-Heidepriem, D. Ehrt, Determination of the OH content of glasses Glastechnische Berichte-Glass Science and Technology, 68, 1995, 139-146.
40. L.L. Velli, C.P.E. Varsamis, E.I. Kamitsos, D. Möncke, D. Ehrt, Optical basicity and refractivity in mixed oxyfluoride glasses, Phys. Chem. Glasses – Eur. J. Sci.. Technol. B, 49, 2008, 182-187.
41. J.A. Duffy, A common optical basicity scale for oxide and fluoride glasses, J. Non-Cryst. Solids, 109, 1989, 35-39, https://doi.org/10.1016/0022-3093(89)90438-9
42. J.A. Duffy, Optical basicity of fluorides and mixed oxide-fluoride glasses and melts, Phys. Chem. Glasses – Eur. J. Sci.. Technol. B, 52, 2011, 107-114.
43. D. Möncke, E.I. Kamitsos, D. Palles, R. Limbach, A. Winterstein-Beckmann, T. Honma, Z. Yao, T. Rouxel, L. Wondraczek, Transition and post- transition metal ions in borate glasses: Borate ligand speciation, cluster formation and their effect on glasstransition and mechanical properties, The Journal of Chemical Physics, 145, 216, 124501, http://dx.doi.org/10.1063/1.4962323.